DOI: 10.1002/ejic.200901174

Comparative Solution Equilibrium Study of the Interactions of Copper(II), Iron(II) and Zinc(II) with Triapine (3-Aminopyridine-2-carbaldehyde Thiosemicarbazone) and Related Ligands

Éva A. Enyedy,*[a] Nóra V. Nagy,[b] Éva Zsigó,[a] Christian R. Kowol,*[c] Vladimir B. Arion,[c] Bernhard K. Keppler,[c] and Tamás Kiss[a]

Keywords: Antitumor agents / Stability constants / EPR spectroscopy / Transition metals / Thiosemicarbazones

The interactions of Cu^{II}, Zn^{II} and Fe^{II} with Triapine (3-aminopyridine-2-carbaldehyde thiosemicarbazone), which is currently undergoing phase II clinical trials as a chemotherapeutic antitumour agent, were investigated in a water/DMSO mixture. The proton-dissociation constants of the ligands, the stability constants and the coordination modes of the metal complexes formed were determined by pH-potentiometric, UV/Vis spectrophotometric, EPR, ^{1}H NMR spectroscopic and ESI-MS methods. Two N-terminally dimethylated derivatives of Triapine were also studied. Mono- and bis-ligand complexes in different protonation states were identified. Furthermore, the formation of the dinuclear species $[Cu_2\mathbf{L}_3]^+$ was confirmed for all ligands by EPR spectroscopy and ESI-MS measurements. The results showed that the N-terminally dimethylated ligands are much more potent chelators than Triapine for the divalent metal ions studied. All three ligands formed the least stable complexes with Zn^{II}, whereas the Fe^{II} complexes were somewhat more stable than the corresponding Cu^{II} species.

Introduction

Thiosemicarbazones (TSCs) are widely applied in analysis, e.g., for the spectrophotometric and spectrofluorimetric detection of various metal ions.[1] Additionally, they possess a broad range of pharmaceutical properties, such as antimalarial, antimicrobial and antitumour activity.[2] α-N-heterocyclic TSCs have been found to exhibit significant antitumour effects, and the most prominent derivative, Triapine (3-aminopyridine-2-carbaldehyde thiosemicarbazone, Scheme 1), which is currently undergoing phase II clinical trials,[3] is a potent inhibitor of ribonucleotide reductase (RR),[4,5] which plays a central role in cell proliferation by supplying deoxyribonucleotide precursors for DNA synthesis and repair. The active subunit of RR consists of a tyrosyl radical cofactor and a nonheme di-Fe centre.[6] The Fe^{II} and Fe^{III} complexes of Triapine are also efficient RR inhibitors, and it has been assumed that the formation of an intracellular Fe complex plays a crucial part in the mechanism of enzyme inhibition.[4,7] The Fe^{II}–Triapine complex is a much more potent inhibitor of isolated RR than the Fe^{III} complex or the metal-free ligand,[4] though cytotoxicity studies on cancer cell lines have shown that the IC_{50} values of Triapine and its Fe complexes are quite similar.[5,7–9] A possible explanation of the differences between the inhibition potency of isolated RR and its cytotoxicity is the lower cell uptake of the positively charged Fe^{III} complex as compared with metal-free Triapine.[8] The mode of action of Fe complexes of α-N-heterocyclic thiosemicarbazones intracellularly is associated with their redox activity. The formal potentials of the reversible Fe^{III}/Fe^{II} redox couple of pyridine TSCs lie within the range of available cellular oxidants and reductants,[8–11] thus allowing the complexes to undergo redox cycling and thereby produce reactive oxygen species under physiological conditions, which can destroy the tyrosyl radical of RR.[4]

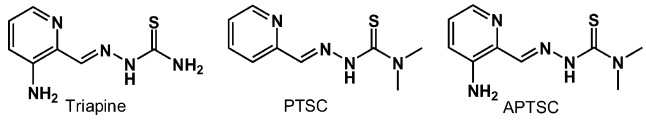

Scheme 1. Ligands used in this study: Triapine = 3-aminopyridine-2-carbaldehyde thiosemicarbazone; PTSC = pyridine-2-carbaldehyde N^4,N^4-dimethylthiosemicarbazone; APTSC = 3-aminopyridine-2-carbaldehyde N^4,N^4-dimethylthiosemicarbazone.

Besides the strong chelating properties toward Fe^{II} and Fe^{III} ions, α-N-heterocyclic TSCs form complexes of high stability with other transition-metal ions too, such as Cu^{II},

[a] Department of Inorganic and Analytical Chemistry, University of Szeged,
P. O. Box 440, 6701 Szeged, Hungary
Fax: +36-62-420505
E-mail: enyedy@chem.u-szeged.hu
[b] Institute of Structural Chemistry,
Chemical Research Center of the Hungarian Academy of Sciences,
Pusztaszeri út 59–67, 1025 Budapest, Hungary
[c] Institute of Inorganic Chemistry, University of Vienna,
Währinger Strasse 42, 1090 Vienna, Austria
E-mail: christian.kowol@univie.ac.at
Supporting information for this article is available on the WWW under http://dx.doi.org/10.1002/ejic.200901174.

Zn^{II}, Ga^{III}, Ru^{II} and Ru^{III}, which likewise possess cytotoxic activity.[8,12,13] Moreover, [Cu^{II}–bis(thiosemicarbazonate)] complexes are currently under investigation as hypoxia-selective positron-emission tomography tracers.[14] TSCs usually coordinate to the metal centre by means of an (N,S) bidentate mode and the binding of both neutral and anionic forms is possible.[15,16] Monodentate coordination through the thione group has also been documented in the case of soft-metal ions such as Ag^{I} and Hg^{II}.[17] When a coordinating functionality is additionally present in the TSC ligand, more diversified binding modes can occur; typically, tridentate (X,N,S) coordination can be found in the octahedral bis-ligand complexes, in which X is the donor atom of the additional functional group. Sulfur too can serve as a bridging ligand to an adjacent metal centre to form dimers (e.g., in the case of Cu^{II}).[18] Numerous dimeric Cu^{II} complexes that contain chloride, bromide, hydroxide, acetate, etc. bridging ligands between two monomeric units have been synthesized and characterized by X-ray crystallography.[15,19]

This wide range of possible coordination modes in the complexes of TSC derivatives is usually reported for compounds in the solid state or in solution with organic solvents; relatively little information is available in the literature on complex-formation processes of TSCs in aqueous solution.[20–23] The generally low solubility of TSCs in water results in experimental limitations for solution equilibrium studies; however, a knowledge of the speciation of metal complexes, especially at physiological pH, can provide information concerning the actual chemical form of the complex in biological media, and this can contribute to a better understanding of the differences in their biological activity. A comparative equilibrium solution study was therefore performed on the complexes of Triapine with the biologically essential transition-metal ions (i.e., Cu^{II}, Fe^{II}, Zn^{II}) in a dimethyl sulfoxide (DMSO)/water mixture by means of pH-potentiometric, UV/Vis spectrophotometric, EPR, ^{1}H NMR spectroscopic and ESI-MS methods. To clarify possible relationships between complex stability and cytotoxic potency, terminally dimethylated derivatives of Triapine (see Scheme 1) were also included in this study.

Results and Discussion

Proton Dissociation Processes

The proton-dissociation processes of the ligands (shown in Scheme 1) were followed by pH-potentiometric, UV/Vis spectrophotometric and ^{1}H NMR spectroscopic titrations. All these ligands are poorly soluble in water, and various DMSO/H_2O solvent mixtures were tested as suitable media for aqueous solution equilibrium studies; 30% (w/w) DMSO/H_2O was found to be sufficient for dissolution of the ligands at the concentration levels necessary for pH-potentiometric titrations (i.e., ≥1–2 mM). The hydrolytic stabilities of the ligands were monitored by a second titration with KOH following back-acidification of the initially titrated sample from pH 2 to 12. The recorded titration curves were almost exactly superimposed: the protonation constants calculated from the two consecutive titrations were found to be equal within ±0.04 log units, which indicates that no decomposition occurred. Protonation constants determined by pH-potentiometric and UV/Vis spectrophotometric methods are reported in Table 1. Two proton-dissociation processes could be determined for the ligands Triapine, pyridine-2-carbaldehyde N^4,N^4-dimethylthiosemicarbazone (PTSC) and 3-aminopyridine-2-carbaldehyde N^4,N^4-dimethylthiosemicarbazone (APTSC), and the constants obtained by the two kinds of method were in reasonably good agreement.

Table 1. Protonation and dissociation constants [$\log\beta(H_iL)$; pK_i] of the ligands studied at t = 25.0 °C, I = 0.10 M (KCl) in 30% (w/w) DMSO/H_2O.[a]

	Triapine	PTSC	APTSC
$\log\beta(HL)$[b]	10.78(1)	10.54(1)	10.29(1)
$\log\beta(H_2L^+)$[b]	14.70(1)	13.92(1)	14.60(1)
pK_1[b]	3.92	3.38	4.31
pK_2[b]	10.78	10.54	10.29
$\log\beta(HL)$[c]	10.86(1)	10.52(1)	10.35(1)
$\log\beta(H_2L^+)$[c]	14.65(1)	13.81(1)	14.60(1)
pK_1[c]	3.79	3.29	4.25
pK_2[c]	10.86	10.52	10.35

[a] Uncertainties (standard deviations, SD) are shown in parentheses for the species determined in the present work. [b] Determined by pH-potentiometry. [c] Determined by UV/Vis spectrophotometric titrations.

UV/Vis spectrophotometric titrations revealed characteristic spectral changes in the 260–450 nm wavelength range. The ligands display two intense absorption bands in this range, which are assigned to n→π* transitions of the pyridine ring and the thiosemicarbazide moiety.[24] Representative spectra for APTSC, together with the individual spectra calculated for the ligand species in different protonation forms, are shown in Figure 1 (a, b). As a consequence of the extended conjugated electronic systems in the ligands, both deprotonation steps are accompanied by changes in the absorption bands. Similar behaviour was observed for all the ligands studied. During the first deprotonation step ([H_2**L**]$^+$ → [H**L**]), a blueshift and a decrease in intensity of the absorption maximum in the visible region of the spectra were observed, whereas the second deprotonation ([H**L**] → [**L**]$^-$) was accompanied by a redshift and an increase in intensity (Figure 1, b).

Protonation constants and the individual spectra for the ligand species [H_2**L**]$^+$, [H**L**] and [**L**]$^-$ (Table 2) were calculated on the basis of deconvolution of UV/Vis spectra recorded at different pH values. UV/Vis titration of 2-formylpyridine thiosemicarbazone in pure aqueous solution resulted in similar proton-dissociation constants and individual spectra.[21,22]

Concentration distribution curves, together with absorbance values at λ_{max} as a function of pH, are reported as Supporting Information (Figure S1).

The pK values determined demonstrate that the proton-dissociation processes do not overlap, and the neutral form [H**L**] predominates in the physiological pH range, as illus-

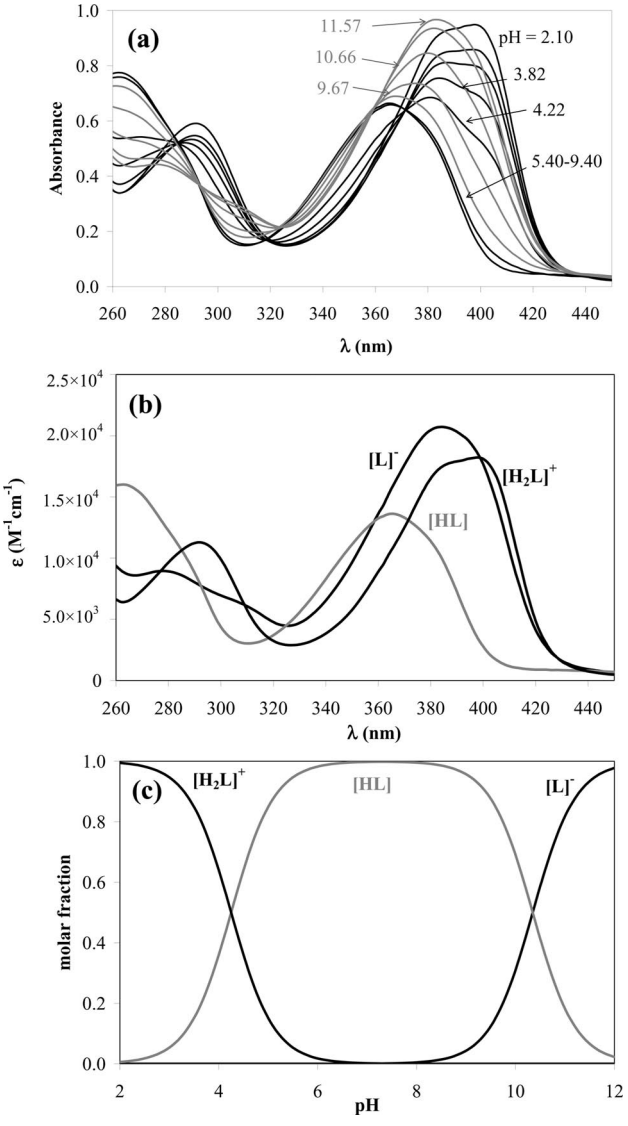

Figure 1. (a) UV/Vis absorption spectra of ligand APTSC recorded at different pH values [c_{ligand} = 0.05 mM; t = 25.0 °C, I = 0.10 M (KCl) in 30% (w/w) DMSO/H_2O]; (b) calculated individual absorption spectra of APTSC species; (c) concentration distribution curves for APTSC species (c_{ligand} = 0.05 mM).

Table 2. λ_{max} [nm] and molar absorptivity [$M^{-1}cm^{-1}$] values (in parentheses) for ligand species $[H_2L]^+$, [HL] and $[L]^-$ determined by UV/Vis spectrophotometric titrations [t = 25.0 °C, I = 0.10 M (KCl) in 30% (w/w) DMSO/H_2O].

	$[H_2L]^+$	[HL]	$[L]^-$
Triapine	402 (20.6×10^3)	368 (15.6×10^3)	376 (17.2×10^3)
	290 (10.8×10^3)	290 (11.5×10^3)	
PTSC	340 (13.0×10^3)	312 (11.7×10^3)	366 (11.3×10^3)
APTSC	398 (18.2×10^3)	366 (13.6×10^3)	384 (20.7×10^3)
	292 (11.3×10^3)		

trated for APTSC in Figure 1 (c). pK_1 can presumably be attributed to deprotonation of the pyridinium unit, and pK_2 to deprotonation of the hydrazinic N^2–H group of the thiosemicarbazide moiety (Scheme 2). Similar behaviour has been described for other TSCs.[20–22] Following deprotonation of the N2–H group, the negative charge is mainly transferred to the S atom via the thione–thiol tautomeric equilibrium (Scheme 2). Protonation of the pyridine N under acidic conditions was confirmed by an X-ray diffraction study of Triapine·HCl·H_2O, the results of which are presented in Figure 2.

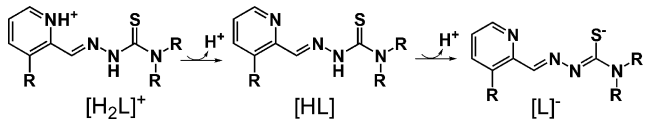

Scheme 2. Deprotonation steps of the thiosemicarbazone ligands.

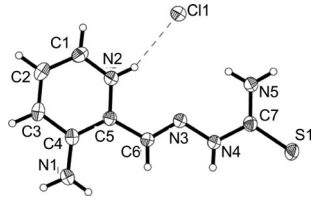

Figure 2. X-ray structure of Triapine·HCl·H_2O (the water molecule is omitted and the thermal ellipsoids are drawn at 30% probability level).

The effects of various substituents on the proton-dissociation constants are worthy of mention. The electron-donating amino group at C3 of the pyridine ring increases pK_1, whereas the methyl groups on the terminal N slightly decrease pK_2 (Table 1).

Additionally, the proton-dissociation processes of the TSCs were monitored by ^{1}H NMR spectroscopic titration. The chemical shifts (δ) of certain protons exhibited reasonable sensitivity to the protonation state of the ligand, as shown for Triapine in Figure 3. The chemical shifts of the different Triapine species, determined by deconvolution of the ^{1}H NMR spectra, are to be seen in Table S1 in the Supporting Information. Despite the presence of two distinct protonation sites, electronic deshielding effects were observed for all monitored signals, presumably due to the conjugated electronic system of the ligands. Upon deprotonation of the pyridinium group (between pH ≈ 3 and 5), upfield shifts were observed for all the protons of the pyridine ring, whereas the protons *meta* and *para* to the pyridine N proved to be the most sensitive. Further upfield shifts of the δ values of the CH protons of the ring occurred when the second proton-dissociation step took place at the TSC moiety, whereas the signal of the CH(=N) proton, which is located closest to the second protonation site (N2–H), demonstrated only a slight downfield shift. The terminally dimethylated derivatives (PTSC and APTSC) possess lower solubility, which resulted in lower-quality spectra; therefore, we followed only the signals of the *N*-methyl protons with some degree of certainty, and moderate upfield shifts of δ were observed as the first and second deprotonation steps (see Figures S2 and S3 in the Supporting Information) took place.

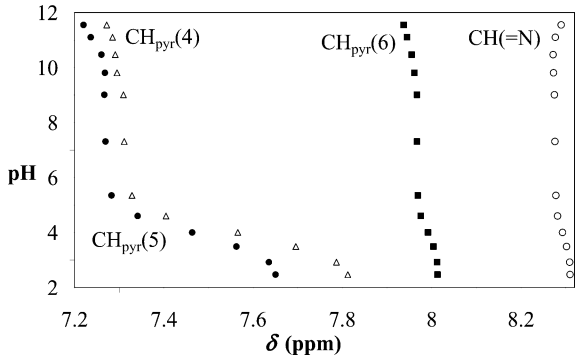

Figure 3. pH-dependent chemical shifts [ppm] for Triapine protons measured by ^{1}H NMR spectroscopic titration {t = 25.0 °C in 30% (w/w) [D_6]DMSO/D_2O}.

Complex Formation with Divalent Metal Ions

The complex formation processes of Triapine, PTSC and APTSC with Cu^{II}, Zn^{II} and Fe^{II} were studied by pH potentiometry in a 30% (w/w) DMSO/H_2O solvent mixture. The experimental titration data indicated that these ligands were efficient metal-ion chelators in a wide pH range for all three metal ions. It should be noted, however, that the ligands were not able to keep the metal ions in solution at a metal-to-ligand ratio of 1:1 at highly basic pH, and precipitation occurred. The complex formation processes with all three ligands start at low pH (pH ≈ 2) in the case of Cu^{II} and Fe^{II}; the representative titration curves for Triapine show this in Figure 4. Complexation of Zn^{II} with Triapine proceeds only at pH > 4, whereas interactions between Zn^{II} and the terminally dimethylated ligands, PTSC and APTSC, are observed at significantly lower pH. Formation of non-negligible amounts of mixed hydroxido species occurred at basic pH, as concluded from the base consumption exceeding the number of dissociable protons in the ligands.

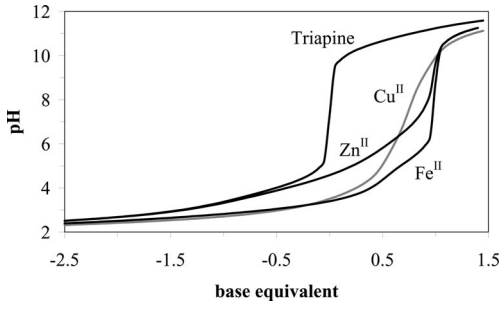

Figure 4. Representative pH-potentiometric titration curves for Triapine, Cu^{II}–Triapine, Zn^{II}–Triapine and Fe^{II}–Triapine systems [c_{ligand} = 2 mM; M/**L** = 1:2; t = 25.0 °C, I = 0.10 M (KCl) in 30% (w/w) DMSO/H_2O]. Negative base equivalent values mean an excess amount of acid.

The stoichiometries of the metal complexes and the stability constants furnishing the best fits to the pH-potentiometric experimental data together with some stepwise and derived equilibrium constants are listed in Table 3. The data reveal the formation of mono-ligand complexes such as $[M\mathbf{L}H]^{2+}$, $[M\mathbf{L}]^{+}$, $[M\mathbf{L}H_{-1}]$ and $[M\mathbf{L}H_{-2}]^{-}$ and bis-ligand complexes such as $[M\mathbf{L}_2H]^{+}$, $[M\mathbf{L}_2]$ and $[M\mathbf{L}_2H_{-1}]^{-}$. The EPR spectroscopy measurements and the ESI-MS findings indicated that Cu^{II} is prone to form dinuclear species (e.g. $[M_2\mathbf{L}_3]^{+}$), which were included in the accepted models. In the protonated mono and bis complexes, the protons can presumably be attributed to the noncoordinating hydrazinic N2 atom and coordination through the (N_{pyr},N1, S) donor set can be suggested, as depicted in Scheme 3 for the octahedral Zn^{II} and Fe^{II} complexes. This mode of coordination was recently confirmed by an X-ray diffraction study of $[Zn(H\mathbf{L})Cl_2]HCl$ in the case of Triapine.[25] The species $[M\mathbf{L}]^{+}$ and $[M\mathbf{L}_2]$ most probably contain ligands coordinated to Fe^{II} and Zn^{II} through the (N_{pyr},N1,S^{-}) donor set, as illustrated in Scheme 3. This is the typical coordination mode for the pyridinecarbaldehyde TSCs.[15]

Table 3. Stability constants [$\log\beta(M_pL_qH_r)$] for the divalent metal complexes of the TSC ligands with some stepwise and derived constants at t = 25.0 °C, I = 0.10 M (KCl) in 30% (w/w) DMSO/H_2O.[a]

	Triapine	PTSC	APTSC
$\log\beta([Cu\mathbf{L}]^{+})$	13.89(3)	13.57(2)	13.95(2)
$\log\beta([Cu\mathbf{L}H_{-1}])$	5.89(7)	–	7.20(7)
$\log\beta([Cu\mathbf{L}H_{-2}]^{-})$	–5.98(7)	–	–
$\log\beta([Cu\mathbf{L}_2H]^{+})$	27.16(9)	27.49(3)	28.11(3)
$\log\beta([Cu\mathbf{L}_2])$	20.32(8)	21.23(5)	21.90(5)
$\log\beta([Cu_2\mathbf{L}_3]^{+})$	38.79(12)	39.00(10)	41.12(6)
fitting parameter [mL]	2.44×10^{-3}	1.46×10^{-3}	2.03×10^{-3}
$\log K([Cu\mathbf{L}_2])$	6.43	7.66	7.95
$\log\{K([Cu\mathbf{L}]^{+})/K([Cu\mathbf{L}_2])\}$	7.46	5.91	6.00
$\log\beta([Cu\mathbf{L}]^{+}) - \log\beta(H_2\mathbf{L})$[b]	–0.81	–0.35	–0.65
$\log\beta([Cu\mathbf{L}_2]) - 2\times\log\beta(H_2\mathbf{L})$[b]	–9.08	–6.61	–7.30
pCu[c]	10.73	10.87	12.33
$\log\beta([Zn\mathbf{L}H]^{2+})$	13.25(2)	–	14.56(4)
$\log\beta([Zn\mathbf{L}]^{+})$	8.78(1)	12.56(5)	10.34(4)
$\log\beta([Zn\mathbf{L}_2H]^{+})$	21.83(8)	–	–
$\log\beta([Zn\mathbf{L}_2])$	16.26(2)	20.81(8)	17.17(9)
$\log\beta([Zn\mathbf{L}_2H_{-1}]^{-})$	4.57(2)	–	–
fitting parameter [mL]	1.17×10^{-3}	2.67×10^{-3}	2.07×10^{-3}
$\log K([Zn\mathbf{L}_2])$	7.48	8.25	6.83
$\log\{K([Zn\mathbf{L}]^{+})/K([Zn\mathbf{L}_2])\}$	1.30	4.31	3.51
$\log\beta([Zn\mathbf{L}]^{+}) - \log\beta(H_2\mathbf{L})$[b]	–5.92	–1.36	–4.26
$\log\beta([Zn\mathbf{L}_2]) - 2\times\log\beta(H_2\mathbf{L})$[b]	–13.14	–7.03	–12.03
pZn[c]	5.28	9.27	7.30
$\log\beta([Fe\mathbf{L}H]^{2+})$	15.91(2)	–	–
$\log\beta([Fe\mathbf{L}]^{+})$	12.29(3)	13.27(1)	14.37(4)
$\log\beta([Fe\mathbf{L}H_{-1}])$	–	–	8.92(5)
$\log\beta([Fe\mathbf{L}_2H]^{+})$	27.70(3)	27.54(2)	29.09(5)
$\log\beta([Fe\mathbf{L}_2])$	22.55(5)	23.37(2)	24.16(5)
$\log\beta([Fe\mathbf{L}_2H_{-1}]^{-})$	10.83(9)	–	–
fitting parameter [mL]	3.73×10^{-3}	2.23×10^{-3}	4.17×10^{-3}
$\log K([Fe\mathbf{L}_2])$	10.26	10.10	9.79
$\log\{K([Fe\mathbf{L}]^{+})/K([Fe\mathbf{L}_2])\}$	2.03	3.17	4.58
$\log\beta([Fe\mathbf{L}]^{+}) - \log\beta(H_2\mathbf{L})$[b]	–2.41	–0.65	–0.23
$\log\beta([Fe\mathbf{L}_2]) - 2\times\log\beta(H_2\mathbf{L})$[b]	–6.85	–4.47	–5.04
pFe[c]	8.76	9.98	13.14

[a] Uncertainties (SD) are shown in parentheses for the complexes determined in the present work. [b] For the values see Table 1. [c] pM (= $-\log[M^{2+}]$) values at pH = 7.25 (pK_w = 14.5); c_{ligand} = 1 mM; M/**L** = 1:2.

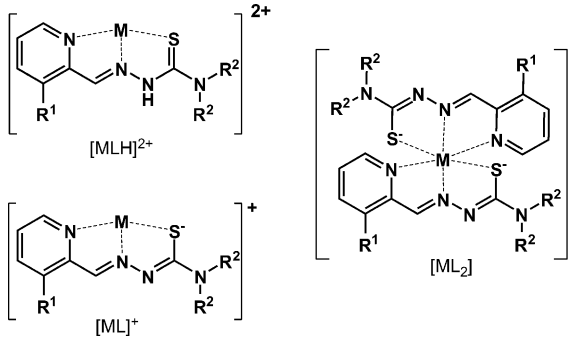

Scheme 3. Proposed structures for $[ML H]^{2+}$, $[ML]^{+}$ and $[ML_2]$ Fe^{II} and Zn^{II} complexes.

The species $[ML H_{-1}]$, $[ML H_{-2}]^{-}$ and $[ML_2 H_{-1}]^{-}$ formed at basic pH should be regarded as mixed hydroxido complexes $[ML(OH)]$, $[ML(OH)_2]^{-}$ and $[ML_2(OH)]^{-}$, which result from the deprotonation of coordinated water molecules. In some cases, mixed hydroxido species could not be detected because precipitation occurred in the pH range of their formation. The Cu^{II} complexes exhibited somewhat different behaviour, as they possess octahedral geometry with tetragonal distortion due to the Jahn–Teller effect; their coordination modes are discussed in a separate section below.

The thermodynamic stabilities of the metal complexes formed with the different ligands can be compared by various modes (e.g., considering merely the $\log\beta[ML]$ and $\log\beta[ML_2]$ values in the case of a certain metal ion), although derived constants for the reactions below can give further information relating to the stabilities of the metal chelates. Higher derived constants imply more favoured metal complex formation as compared with that for the proton complex.

$$M^{2+} + H_2L^{+} \rightleftharpoons [ML]^{+} + 2H^{+} \quad \{\log K = \log\beta([ML]^{+}) - \log\beta(H_2L^{+})\}$$

$$M^{2+} + 2H_2L^{+} \rightleftharpoons [ML_2] + 4H^{+} \quad \{\log K = \log\beta([ML_2]) - 2\times\log\beta(H_2L^{+})\}$$

The derived constants in Table 3 reveal that PTSC and APTSC are much more effective chelators than Triapine for Zn^{II}, Fe^{II} and Cu^{II}; the data are especially high in the case of PTSC. For biologically active metal complexes, ligand preference is of particular interest at physiological pH; it can be expressed by comparison of the concentrations of the free metal ion in different metal–ligand systems. These values reveal how efficiently the ligand can keep the metal ion in complexed forms even in different species. For this reason, pM values were calculated at neutral pH (Table 3). It can be seen that Triapine always has the lowest pM values and APTSC is the most efficient metal binder for Cu^{II} and Fe^{II}, whereas PTSC is the most efficient for Zn^{II}.

It may be concluded from all these findings that the presence of the methyl groups on the terminal amino N of pyridinecarbaldehyde TSCs results in more favourable complex formation than that with the terminally unsubstituted TSCs such as Triapine.

As concerns the sequence of the stability constants for the metal complexes formed in the M^{II}–TSC systems (e.g., $\log\beta[ML]$ and $\log\beta[ML_2]$ in Table 3), it may be seen that Zn^{II} forms the least stable complexes and the species formed with Fe^{II} are usually somewhat more stable than those of Cu^{II}. This trend is not in accordance with the Irving–Williams series, most probably because of the formation of low-spin Fe^{II} complexes with marked stability due to the (N_{pyr},N,S^{-}) coordination mode.[13] This environment provides moderate formal potentials for the reversible $[Fe^{III}L_2]^{+}/[Fe^{II}L_2]$ redox couples at physiological pH [e.g., for L = Triapine, PTSC and APTSC; $E°' = +0.07$, +0.14 and +0.05 V, respectively, vs. NHE in 30% (w/w) DMSO/H_2O, $t = 25.0$ °C, $I = 0.10$ M (KCl)[26]]. It is noteworthy that the stepwise stability constants exhibit the usual sequence: $\log K([ML]^{+})$ is always higher than $\log K([ML_2])$, whereas the $\log\{K([ML]^{+})/K([ML_2])\}$ values are several orders of magnitude higher for Cu^{II} than for Zn^{II} and Fe^{II}, thus indicating the less favoured coordination of the second ligand in the Cu^{II} complexes.

Spectroscopic methods such as EPR spectroscopy for the Cu^{II} complexes, ^{1}H NMR spectroscopy for the Zn^{II} systems, and UV/Vis spectrophotometry for the Fe^{II} and Cu^{II} systems, were applied to obtain further information on the coordination mode and geometry of the complexes of the TSC derivatives.

^{1}H NMR spectra for the Zn^{II}–Triapine system were recorded at different pH values. The signals of the metal-free and complexed ligand could not be distinguished due to the fast proton- and ligand-exchange processes. The changes in the chemical shifts of CH(=N) and the CH protons of the pyridine ring were therefore monitored as a function of pH to ascertain the stability constants. In the presence of Zn^{II}, the changes were similar to those as in the case of the second deprotonation step of the metal-free ligand. Upfield shifts of the signals of the pyridine ring protons and a downfield shift of that of the CH(=N) proton were observed with increasing pH. However, these changes appeared at much lower pH (pH ≈ 5) than in the case of the metal-free ligand as a consequence of proton displacement due to the Zn^{II} complex formation (not shown). Moreover, the changes were found to be more significant for the proton *ortho* to the pyridine N and CH(=N), which are situated closest to the metal centre (e.g., a few tenths of ppm as compared with the free ligand). The formation of the joint chelate rings also seems to play a role. It is worth noting that the N-terminal methyl protons of PTSC in the presence of Zn^{II} revealed a considerable upfield shift above pH 3, thus indicating that the complex formation starts at much lower pH with this ligand than with Triapine, as a consequence of the higher stability species (Figures S2 and S3 in the Supporting Information).

UV/Vis spectrophotometric measurements under strictly anaerobic conditions at different pH values were performed to gain a better insight into the formation of Fe^{II} complexes with the TSC ligands; the results for the Fe^{II}–Triapine system are shown in Figure 5. The concentration distribution curves reflect the pH-dependent formation of the different

Fe^{II} species (inset of Figure 5). The UV/Vis spectra of quite dilute solutions [$c(Fe^{II})$ = 0.03 mM] were recorded, because of the intense colours of the metal complexes. During the titrations, the solutions changed from red at low pH to bluish-green at pH ≈ 4–5 and to green at above pH ≈ 7. In the case of Triapine, broad absorption bands were observed in the region 450–680 nm due to the complex formation (the terminally dimethylated ligands behaved similarly). As the metal-free ligand does not absorb in this region, these are most probably charge-transfer (CT) bands of the Fe^{II} complexes. The formation of mono complexes resulted in a shoulder in the interval 450–500 nm, whereas formation of the bis-ligand species was accompanied by the development of an absorption band with maximum at 620 nm. The spectra recorded between pH 6.8 and 10 corresponded to the spectrum of the complex [Fe$\mathbf{L}_2$] as also reported by Shao et al.[4] The (N_{pyr},N,S^-) donor set and especially the coordination of the aromatic nitrogen atoms in the complexes [Fe$\mathbf{L}_2$] resulted in CT bands with high molar absorptivity in the visible region. This donor set in the complex also led to a certain stabilization of the lower oxidation state {see $E°'([Fe^{III}\mathbf{L}_2]^+/[Fe^{II}\mathbf{L}_2])$ values above}.

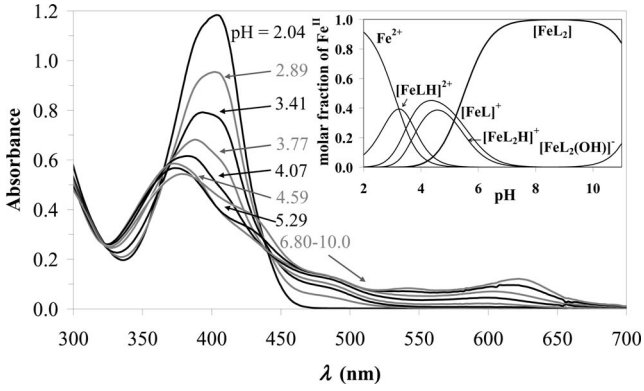

Figure 5. UV/Vis absorption spectra of Fe^{II}–Triapine system recorded at different pH values [c_{ligand} = 0.06 mM; M/**L** = 1:2; t = 25.0 °C, I = 0.10 M (KCl) in 30% (w/w) DMSO/H_2O]; Inset: Concentration distribution curves of Fe^{II} complexes formed in the Fe^{II}–Triapine system at metal-ion-to-ligand ratio 1:2, c_{ligand} = 0.06 mM.

Copper(II) Complexes: UV/Vis Spectrophotometric, EPR and ESI-MS Measurements

Complex formation in the Cu^{II}–TSC systems was followed by UV/Vis spectrophotometric and EPR spectroscopic titrations. Representative UV/Vis spectra are presented in Figure 6 (a) for the Cu^{II}–Triapine system. Considerable absorption occurred in the visible region at wavelengths higher than 460 nm for all the TSCs studied. This band is undoubtedly not associated with ligand absorption. An absorption maximum at approximately 650 nm with relatively low molar absorptivity (ε) was observed in the spectra measured at acidic pH, which can be attributed to the d–d transition of the Cu^{II} complexes.[27] The shoulder peak in the interval around 460–600 nm became more intense as the pH was increased, reaching maximal intensity at pH ≈ 8, and then decreases at 554 nm in parallel with the concentration distribution curves (Figure 6, b). This shoulder is probably due to the S–Cu^{II} ligand-to-metal CT band which is present throughout the whole pH range and has a much higher ε value than that of the d–d bands.

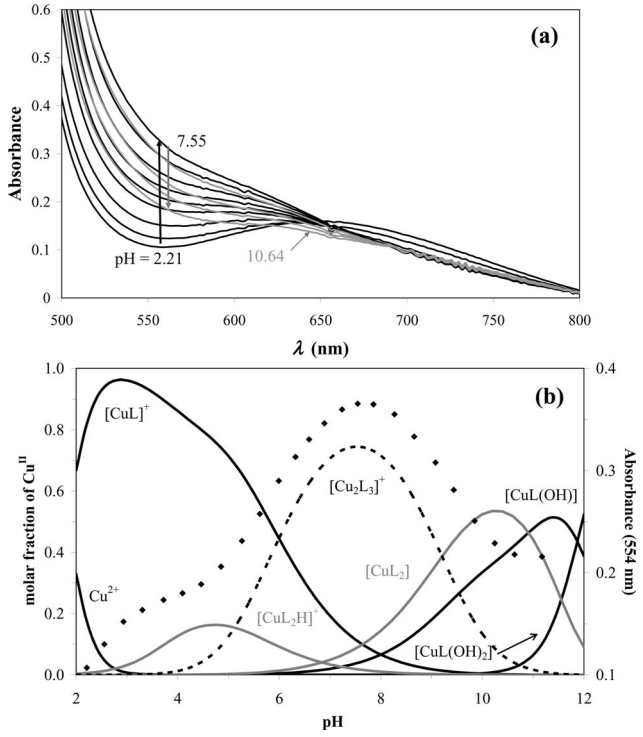

Figure 6. (a) UV/Vis absorption spectra of Cu^{II}–Triapine system recorded at different pH values. (b) Concentration distribution curves of Cu^{II} complexes formed in the Cu^{II}–Triapine system and pH dependence of absorbance values at 554 nm (♦) [$c(Cu^{II})$ = 1 mM; M/**L** = 1:2; t = 25.0 °C, I = 0.10 M (KCl) in 30% (w/w) DMSO/H_2O].

The EPR spectra and their changes at different pH values were found to be quite similar for the three Cu^{II}–TSC systems. The fits between the experimental and the simulated spectra are depicted in Figure 7 using the example of PTSC as ligand, and the isotropic EPR spectroscopic data obtained from the "two-dimensional" simulation are given in Table 4. The component EPR spectra calculated from the simulation are shown in Figure 8. (For the concentration distribution curve data calculated with the stability constants obtained from the EPR spectra simulations, see Table 4 and Figure S8.) These spectroscopic measurements allowed the following conclusions concerning the formation of the Cu^{II} complexes of the TSCs.

Similar speciation models emerged from the EPR spectra simulation as in the case of pH potentiometry, though some differences were also found: the formation of [Cu**L**H]$^{2+}$ and isomers of [Cu$\mathbf{L}_2$H]$^+$ and [Cu$\mathbf{L}_2$] was detected. Both the UV/Vis and the EPR spectra suggested that below pH 3 the presence of the free Cu^{II} ion is almost negligible and the Cu^{II} mostly exists as [Cu**L**H]$^{2+}$ and [Cu**L**]$^+$ in contrast to the concentration distribution curves in Figure 6b, calculated from the results of pH potentiometry. This difference

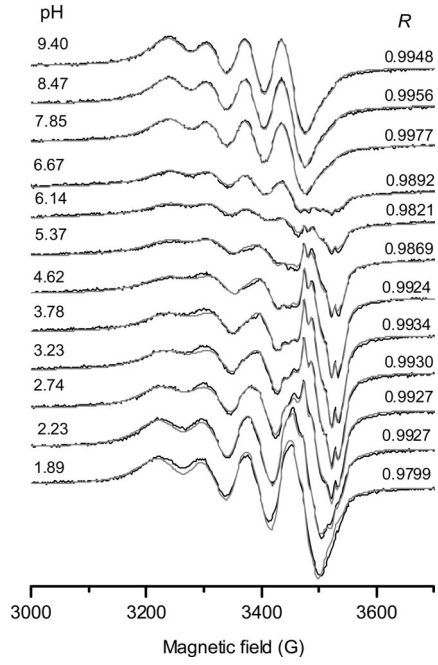

Figure 7. Experimental (black) and simulated (grey) EPR spectra recorded for the Cu^{II}–PTSC system at room temperature. [$c(Cu^{II})$ = 1 mM; M/**L** = 1:2.5; I = 0.10 M (KCl) in 30% (w/w) DMSO/H_2O].

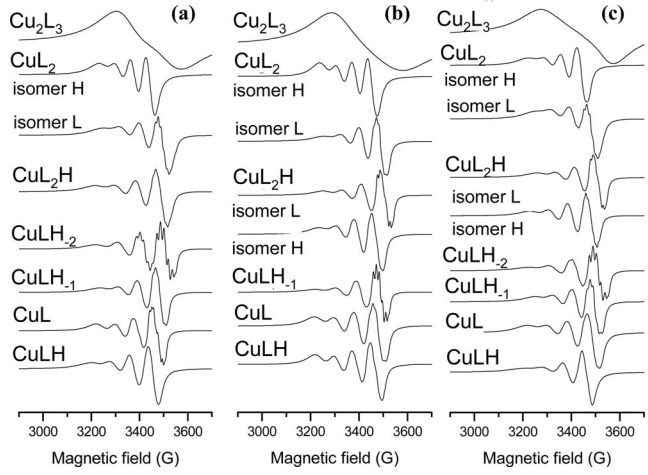

Figure 8. Calculated component EPR spectra obtained for (a) Cu^{II}–Triapine, (b) Cu^{II}–PTSC and (c) Cu^{II}–APTSC (c) systems. Charges of the complexes are omitted for simplicity.

can be explained by the fact that H**L** coordinates to the Cu^{II} ion without deprotonation so that pH potentiometry is not sensitive to its formation, whereas the EPR spectra of the aqua complex of Cu^{II} and $[Cu\mathbf{L}H]^{2+}$ can easily be distinguished. The EPR method can barely distinguish between different constitutions when the EPR parameters are very close (as was found for the highly overlapping $[Cu\mathbf{L}H]^{2+}$, $[Cu\mathbf{L}]^{+}$ and $[Cu\mathbf{L}_2H]^{+}$), and in this case pH potentiometry therefore gives more certain data. Hence, the use of the two different approaches together can yield a reliable description of the systems. Even though a drift in the stability constants was obtained with the two methods,

Table 4. Isotropic EPR spectroscopic parameters of the components obtained for Cu^{II}–Triapine, Cu^{II}–APTSC and Cu^{II}–PTSC systems with overall stability constants of the complexes obtained from the "two-dimensional" simulation of EPR spectra.[a]

	Triapine			PTSC			APTSC		
	g_o A_o [G]	aN [G]	logβ[b]	g_o A_o [G]	aN [G]	logβ[b]	g_o A_o [G]	aN [G]	logβ[b]
Cu^{II}[c]	2.1950 34.0			2.1950 34.0			2.1950 34.0		
$[Cu\mathbf{L}H]^{2+}$	2.1069(3) 73.7(4)	15(7), 10(4)	16.69(2)	2.0977(1) 71.2(2)	14.4(3), 11.3(3)	16.58(2)	2.1010(4) 76.0(6)	14(1), 12.0(5)	17.05(4)
$[Cu\mathbf{L}]^{+}$	2.0958(1) 72.6(1)	16.7(1), 9.8(2)	14.35(2)	2.0943(1) 75.0(2)	16.8(2), 13.4(3)	14.42(2)	2.0903(3) 75.8(3)	17.0(3), 13.1(4)	15.12(4)
$[Cu\mathbf{L}H(OH)]^{+}$	2.0865(4) 70.7(5)	14.1(6), 10.8(5)	4.68(3)	2.0894(1) 77.5(1)	14.4(1), 11.3(1)	4.55(4)	2.0850(3) 70.0(5)	15.2(5), 13.1(3)	5.63(4)
$[Cu\mathbf{L}H(OH)_2]$	2.0826(1) 83.0(2)	17.6(3), 14.3(3)	–7.57(3)				2.0808(2) 82.7(3)	18.3(4), 13.8(3)	–6.75(6)
$[Cu\mathbf{L}_2H]^{+}$			28.67[d]			29.07[d]			29.63[d]
isomer H	2.0905(3) 77.7(4)	16(3), 12.9(4), 12.9(4)	28.67(3)		15.8(3), 11.1(3) 11.1(3)	28.84(1)	2.0902(2) 72.4(2)	15(3) 10(3) 10(3)	29.31(3)
isomer **L**				2.0750(1) 72.9(1)	15.6(1), 10.0(2)	28.70(1)	2.0718(2) 71.4(2)	15.9(3) 10.4(4)	29.35(3)
$[Cu\mathbf{L}_2]$			20.95[d]			22.76[d]			22.40[d]
isomer H	2.1029(4) 60.3(5)	12(1), 6.9(6)	20.64(1)	2.0981(2) 61.2(2)	12.5(5), 8.0(3)	22.70(3)	2.1059(2) 62.0(2)	13.8(3), 11.7(5)	22.28(3)
isomer **L**	2.0796(3) 70.5(3)	12.8(5), 12.8(5), 12.7(5)	20.66(2)	2.0800(6) 66.8(8)	12.8, 12.8, 12.7	21.88(3)	2.083(1) 64.0(8)	12.8 12.8, 12.7	21.78(3)
$[Cu_2\mathbf{L}_3]^{+}$	2.049(2) 55(9)		39.50(9)	2.049(1) 68(6)		42.24(8)	2.058(3) 73(5)		42.95(9)

[a] Uncertainties of the last digits are shown in parentheses. [b] For the proton complexes the pH-potentiometric formation constants in Table 1 were used in the EPR analysis. [c] Fixed values obtained from separate measurements of Cu^{II} without the ligands. [d] $\log\beta = \log(\beta_{\text{isomer L}} + \beta_{\text{isomer H}})$.

the distribution curves are comparable [cf. Figures 6 (b) and S8]. However, the EPR spectrum of $[CuLH]^{2+}$ is not well resolved (N superhyperfine splitting was not clearly detected) in any of the systems; the coordination of the two N atoms (N_{pyr} and N) and the thioamide S can be suggested because of the very low g_o (2.0977–2.1069) and high A_o (71.2–76.0 G) values, which show a very high ligand field (see Table 4) and the appearance of the S–Cu^{II} ligand-to-metal CT bands at low pH values in the UV/Vis spectra. In comparison, for the complex $[CuLH_{-1}]$ of glycyl-L-histidine (N_{im},N_{amid},NH_2), g_o = 2.1143 and A_o = 77.2 G were measured.[28] The slight differences between the parameters of the complexes $[CuLH]^{2+}$ of the three different TSC ligands can be related to their slightly different basicities.

In the case of the complex $[CuL]^+$, a further decrease in g_o was observed for all three TSC ligands, which agrees with the deprotonation of the noncoordinating NH group and coordination through (N_{pyr},N,S^-) is suggested. Slightly resolved N peaks were observed, the best description of which was obtained by taking into account one larger (≈ 16–17 G) and one smaller (≈ 10–13 G) coupling constant. The splitting of two nonequivalent N atoms (a_{N1xx} = 12.7 G, a_{N1yy} = 17.9 G, a_{N1zz} = 10.4 G and a_{N1xx} = 12.4 G, a_{N1yy} = 12.4 G, a_{N1zz} = 14.7 G) was also observed in the spectra recorded at 77 K for the Cu^{II}–PTSC system at pH 3.36, which is probably the spectrum of the $[CuL]^+$ (Figure S6 in the Supporting Information). The unusually high aN_{1yy} value (17.9 G), which can probably be assigned to the central N in the two chelate rings, reflects a high covalency for the N–Cu^{II} σ bond. Furthermore, the anisotropic data (g_{xx} = 2.020, g_{yy} = 2.052, g_{zz} = 2.200 and A_{xx} = 24.9 G, A_{yy} = 22.6 G, A_{zz} = 166.0 G) with $g_{zz} > g_{xx}$, $g_{yy} > 2.040$ suggest that the complex has a $d_{x^2-y^2}$ ground state, characteristic of Cu^{II} complexes with D_{4h} symmetry, but the difference between g_{xx} and g_{yy} demonstrated a strong rhombic distortion of the symmetry in this complex.[29] The EPR parameters of [CuL(OH)] and $[CuL(OH)_2]^-$ agree well with the fact that in the former the water molecule in the equatorial plane is deprotonated, and then another one in the axial position.

Two isomers could be detected for the bis-ligand complexes ($[CuL_2H]^+$ and $[CuL_2]$) with very different g_o values. For simplicity, the isomers were referred to as *L* and *H*, in accord with the lower and the higher g_o values, respectively. However, for $[CuL_2H]^+$, when **L** = Triapine the component with the lower g_o value could not be detected (see Table 4).

The isotropic EPR parameters and the spectra simulation for the $[CuL_2H]^+$ species permitted the conclusion that most probably two and three N-donor atoms are coordinated to Cu^{II} in the equatorial plane in the *L* and *H* isomers of $[CuL_2H]^+$, respectively. Furthermore, the ligand-to-metal CT band can also be seen in the pH range of the formation of this protonated bis-ligand complex in the UV/Vis spectra. The S-donor atom is most likely coordinated to Cu^{II}, and therefore one possible explanation is that ligand L^- is bound through (N_{pyr},N,S^-) and HL is bound in a monodentate manner through (S^-) in the *L* isomer or through N_{pyr} in the *H* isomer of $[CuL_2H]^+$.

Between pH 5 and 10, a species with a very broad EPR signal was detected for all three Cu^{II}–TSC systems. This broadening can be explained by the dipolar interaction of close Cu^{II} centres. The pH-potentiometric and EPR data could be fitted well when the formation of dimeric complexes $[Cu_2L_3]^+$ was presumed and included in the speciation model. In these complexes, the third ligand may link two $[CuL]^+$ moieties as a bridging ligand; however, it is difficult to establish the exact coordination mode on the basis of the EPR and UV/Vis photometric measurements alone. To confirm the formation of $[Cu_2L_3]^+$, electrospray ioniza-

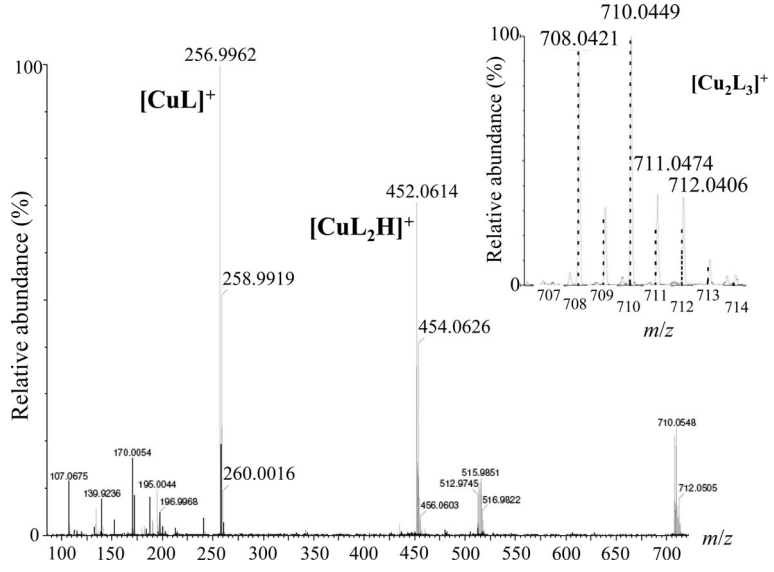

Figure 9. ESI-MS fragmentation spectrum (MS/MS) of the parent peak of $[Cu_2L_3]^+$ at *m/z* 708 recorded in Cu^{II}–Triapine system. Inset: Zoom scan spectrum of the peak attributed to the dimeric $[Cu_2L_3]^+$ complex with its calculated isotopic distribution pattern (dashed line) for the composition of $[Cu_2C_{21}H_{24}N_{15}S_3]^+$ ($c_{Triapine}$ = 0.10 mM; M/L = 1:2; pH = 7.40).

tion mass spectra were recorded for the Cu^{II}–Triapine system at physiological pH: signals of the species $[H_2L]^+$, $[CuL]^+$ and $[CuL_2H]^+$ were detected and also of the dimeric complex $[Cu_2L_3]^+$ (Figure S7 in the Supporting Information). However, it is worth noting that the ESI-MS method does not afford a quantitative picture of the speciation, and only the metal-to-ligand stoichiometry can be obtained (the original number of protons in the complex can not be given due to the proton-transfer reactions activated by the ESI method). A collision-induced fragmentation experiment was performed for the precursor complex $[Cu_2L_3]^+$; the spectrum is shown in Figure 9, in which the inset presents the measured and calculated isotropic pattern of this dimeric species. Fragmentation results in the appearance of the monomeric complexes $[CuL]^+$ and $[CuL_2H]^+$, which are the most probable fragment ions of the species $[Cu_2L_3]^+$.

In the case of the complexes $[CuL_2]$, very different EPR parameters were found for the *L* and *H* isomers, which suggests a completely different arrangement of the donor groups; nevertheless, the assignment is very difficult. The literature contains some data on bis-ligand complexes of TSCs with the $(N,S^-)(N,S^-)$ coordination set, but they are rather contradictory. For example, for pyruvic acid thiosemicarbazone, the parameters $g_\perp = 2.04$ and $g_\parallel = 2.191$ ($g_o = 2.090$) were found for such a bis-ligand complex,[30] whereas a similar structure was suggested for acetophenone thiosemicarbazone when the parameters $g_\perp = 2.04$ and $g_\parallel = 2.158$ ($g_o = 2.079$) were measured.[31] However, the number of possible bis complexes is rather high, as different combinations of the $(N_{pyr},N,S^-)(N \text{ or } S^-)$ or $(N_{pyr},N)(N,S^-)$ coordination sets are also possible in the equatorial plane. For the PTSC, the isomer *H* predominates at pH 9.70; an EPR spectrum was also measured at 77 K (Figure S6) for this complex, with the parameters $g_\perp = 2.046$, $g_\parallel = 2.199$, $A_\perp = 20.1$ G and $A_\parallel = 160.2$ G, similar to those measured for pyruvic acid thiosemicarbazone.[30] Hence, $(N,S^-)(N,S^-)$ coordination is feasible.

For the minor, *L* isomer of Triapine, the isotropic spectra displayed well-resolved N splitting, which could be fitted satisfactorily by taking into account the coordination of three or four N atoms, but the fit was not acceptable with the assumption of only two N-donor atoms. The $(N,S^-)(N_{pyr},N)$ or $(N_{pyr},N)(N_{pyr},N)$ coordination modes in the equatorial plane are therefore more likely for the *L* isomer. It should be noted that the small amount of *L* isomer for PTSC and APTSC allowed only the g_o, A_o and $\log\beta$ data to be fitted for this isomer; other parameters (linewidth parameters and N couplings) were fixed through data obtained for Triapine.

Conclusion

Two general trends were observed in this study: (1) the terminal dimethylation of α-N heterocyclic TSCs results in distinctly increased complex stability as compared with terminally unsubstituted TSCs; (2) comparison of the stabilities of the metal complexes formed with the different divalent metal ions reveals that the Zn^{II} complexes have the lowest stability, and Fe^{II} forms similar, but somewhat more stable complexes than those of Cu^{II}. It was also concluded that the formation of bis-ligand complexes is favourable with Fe^{II} and Zn^{II}, whereas Cu^{II} tends to form the dimeric complexes $[Cu_2L_3]^+$ in the physiological pH range.

As the bis-ligand complexes $[ML_2]$ are usually applied to study anticancer activity, to obtain a view of the most plausible form of these metal complexes in the biological milieu, concentration distribution curves were calculated at neutral pH at different total concentrations of the bis-ligand complex, as shown in Figure 10. At lower concentration, the fraction of the mono-ligand complexes is increased, but this trend is much less pronounced in the case of Fe^{II} due to the high-stability bis-ligand complexes. In general, the enhanced formation of the mono-ligand complexes in dilute aqueous solution can provide a possibility for interactions with other bioligands during the metabolism.

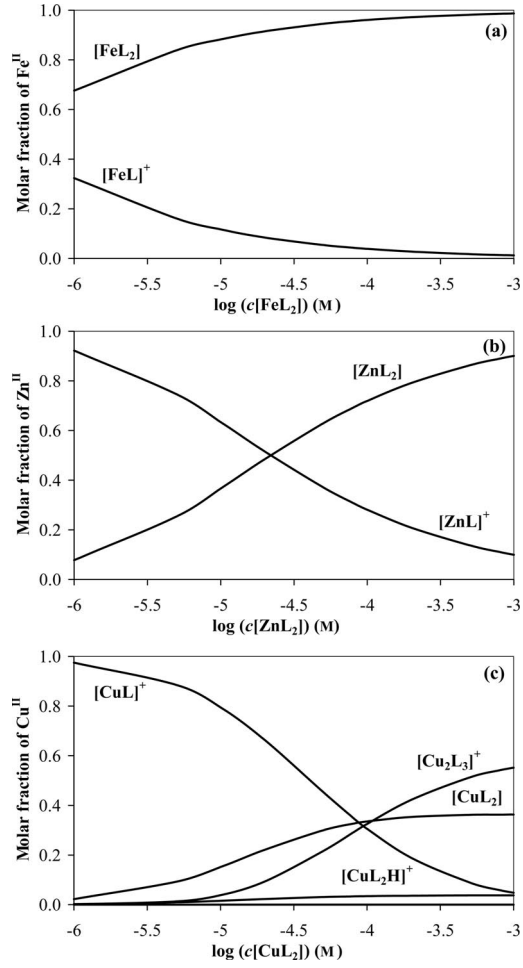

Figure 10. Concentration distribution curves of (a) Fe^{II}, (b) Zn^{II} and (c) Cu^{II} complexes formed in the M^{II}–PTSC systems in relation to the concentration of complex $[ML_2]$ at neutral pH (pH = 7.25; M/L = 1:2; for Triapine, see Figure S9 in the Supporting Information).

As concerns the biological activities of the metal-free ligands, Triapine exhibits IC_{50} values in the low micromolar range; this is followed by the slightly more active APTSC, whereas PTSC exerts strongly enhanced cytotoxic activity in the low nanomolar range.[8] The correlation with the stability constants generally shows that the more active terminally dimethylated TSCs also form the more stable complexes, but the large increase in cytotoxicity from APTSC to PTSC is not reflected by the complex formation strength. However, it must be taken into account that the cytotoxic activity is influenced by a large number of parameters, for example, the lipophilicity, which is certainly lower in the case of APTSC.

Experimental Section

Chemicals: Triapine, PTSC and APTSC were prepared as described previously.[8] The purities and stabilities of the ligands were checked and the exact concentrations of the stock solutions prepared were determined by the Gran method.[32] The Fe^{II} stock solution was obtained from fine Fe powder dissolved in a known amount of HCl solution under a purified, strictly oxygen-free argon atmosphere, then filtered, stored and used under anaerobic conditions. KSCN (Sigma–Aldrich) solution was used to check on the absence of Fe^{III} traces in the Fe^{II} solution. The concentration of the Fe^{II} stock solution was determined by permanganometric titrations under acidic conditions. $CuCl_2$ and $ZnCl_2$ stock solutions were made by the dissolution of anhydrous $CuCl_2$ or of anhydrous $ZnCl_2$ in a known amount of HCl, and their concentrations were determined by complexometry through the EDTA complexes. Accurate HCl concentrations in the Fe^{II} and Zn^{II} stock solutions were determined by pH-potentiometric titration.

pH-Potentiometric Studies: The pH-metric measurements for determination of the protonation constants of the ligands and the stability constants of the metal complexes were carried out at an ionic strength of 0.10 M (KCl, Sigma–Aldrich) at 25.0 ± 0.1 °C in DMSO/water (30:70, w/w) as solvent. The titrations were performed with carbonate-free KOH solution of known concentration (0.10 M). Both the base and the HCl used were Sigma–Aldrich products and their concentrations were determined by pH-potentiometric titration. An Orion 710A pH meter equipped with a Metrohm combined electrode (type 6.0234.100) and a Metrohm 665 Dosimat burette were used for the pH-metric measurements. The electrode system was calibrated according to Irving et al.[33] and the pH-metric readings could therefore be converted into hydrogen-ion concentrations. The average water-ionization constant, pK_w, is 14.520 ± 0.05 with DMSO/water (30:70, w/w) as solvent.[20] The pH-metric titrations were performed in the pH range 2.0–12.0. The initial volume of the samples was 5.0 mL. The ligand concentration was in the range 1–3 mM and metal-ion-to-ligand ratios of 1:1–1:4 were used. The accepted fitting of the titration curves was always less than 0.01 mL. Samples were deoxygenated by bubbling purified argon through them for around 10 min before the measurements. In the case of Fe^{II} samples, argon overpressure was used when Fe^{II} was added to the samples in tightly closed vessels, which were previously completely deoxygenated by bubbling a stream of purified argon through them for approximately 20 min. Argon was also passed above the solutions during the titrations.

The protonation constants of the ligands were determined with the computer program SUPERQUAD;[34] PSEQUAD[35] was utilized to establish the stoichiometry of the complexes and to calculate the stability constants ($\log\beta_{MLH}$). The calculations were always made from the experimental titration data measured before precipitation.

Spectrophotometric Measurements: UV/Vis spectrophotometric titrations were performed on TSCs and Fe^{II}- or Cu^{II}-containing samples; the concentration of ligand was 0.05 mM (for the ligand alone), 0.06 mM (for Fe^{II}–ligand samples) or 1 mM (for Cu^{II}–ligand samples) and the metal-to-ligand ratios were 1:1 and 1:2 in the pH range between 2 and 12 at an ionic strength of 0.10 M (KCl) in 30% (w/w) DMSO/H_2O. For Fe^{II} samples, spectra were recorded under anaerobic conditions. A Hewlett–Packard 8452A diode array spectrophotometer was used to record the spectra in the interval 260–820 nm. The path length was 1 cm. Protonation constants and the individual spectra of the species were calculated by the computer program PSEQUAD.[35]

^{1}H NMR Spectroscopy Measurements: ^{1}H NMR spectroscopic studies were carried out with a Bruker Ultrashield 500 Plus instrument. TSCs were dissolved in a 30% (w/w) [D_6]DMSO/D_2O mixture in a concentration of 1.5 mM and the Zn^{II}-to-ligand ratios were 0:1 and 1:2.

EPR Measurements and Deconvolution of the Spectra: All EPR spectra were recorded with a Bruker EleXsys E500 spectrometer (microwave frequency 9.81 GHz, microwave power 10 mW, modulation amplitude 5 G, modulation frequency 100 kHz). The isotropic EPR spectra were recorded at room temperature in a circulating system. The stock solution contained 1 mM $CuCl_2$ and 2, 2.3 or 2.5 mM Triapine, APTSC or PTSC, in 30% (w/w) DMSO/H_2O for Triapine and PTSC, and in 50% (w/w) DMSO/H_2O for APTSC, at an ionic strength of 0.10 M (KCl). NaOH solution was added to the stock solution to change the pH, which was measured with a Radiometer PHM240 pH/ion Meter equipped with a Metrohm 6.0234.100 glass electrode. A Heidolph Pumpdrive 5101 peristaltic pump was used to circulate the solution from the titration vessel through a capillary tube into the cavity of the instrument. The titrations were carried out under an argon atmosphere. The numbers of spectra recorded during the titration were 15, 16 and 12 for the Cu^{II}–Triapine, Cu^{II}–APTSC and Cu^{II}–PTSC systems, respectively. The pH range covered was 2–12.5 for Triapine and APTSC, and 2–10 for PTSC, as precipitation was observed at higher pH values in the latter case. Measurements were also carried out at 1 mM equimolar metal-to-ligand concentration ratios, but precipitation was observed, which disappeared only at highly basic pH (pH ≈ 11–13). These spectra were also included in the simulation (one spectrum in the case of APTSC, three for PTSC).

For several pH values, some sample (0.10 mL) was taken out of the stock solution and was measured individually in a Dewar that contained liquid nitrogen (at 77 K). Methanol (0.03 mL) was added to the samples to ensure glass formation.

All recorded EPR spectra in the systems were simulated with a spectrum deconvolution method by a computer program. The series of isotropic spectra recorded during a titration were simulated simultaneously by the "two-dimensional" 2D_EPR program.[36] Each component curve was described by the isotropic EPR parameters g_o, A_o and a_N N hyperfine couplings, and the relaxation parameters α, β and γ, which define the line widths through the equation $\sigma_{MI} = \alpha + \beta M_I + \gamma M_I^2$ (in which M_I is the magnetic quantum number of Cu nuclei). The concentrations of the components were varied by fitting the formation constants described by the following general equilibrium:

$$pM + qH + rL \rightleftharpoons M_pH_qL_r$$

$$\beta_{M_pH_qL_r} = \frac{[M_pH_qL_r]}{[M]^p[H]^q[L]^r}$$

in which M denotes the metal ion and **L** the completely deprotonated ligand molecule.

Anisotropic spectra were fitted individually by the EPR program, which gives the anisotropic EPR parameters (g_{xx}, g_{yy}, g_{zz} and A_{xx}, A_{yy}, A_{zz}, aN_{xx}, aN_{yy}, aN_{zz}, and the orientation-dependent linewidth parameters).[37] Of the EPR spectra recorded at 77 K, only two were selected and simulated, under conditions where a dominant complex was formed. In the other cases, the quality of the spectra was not good enough for simulation.

Since natural $CuCl_2$ was used for the measurements, the spectrum of each species was calculated as the sum of the spectra of ^{63}Cu and ^{65}Cu weighted by their natural abundances. The Cu and N coupling constants and the relaxation parameters are given in field dimensions (gauss [G]; 1 G = 10^{-4} T). For each spectrum, the computer programs provide the noise-corrected regression parameter (Rj for the jth spectrum) derived from the average square deviation between the experimental and the calculated spectrum. For the series of spectra, the fit is characterized by the overall regression coefficient R, calculated from the overall average square deviation. The details of the statistical analysis were published previously.[36]

ESI-MS Measurements: ESI-MS spectra were recorded with a Waters Q-TOF Premier instrument (Micromass MS Technologies, Manchester, UK) operating in positive ion mode. Samples were introduced into the ESI source by the syringe pump of the instrument. N_2 was used as nebulizer and cone gas, and the source temperature was set to 120 °C. The capillary voltage was set to 3.8 kV. Argon was employed as the collision gas and the collision energy was –25 eV. The ChemDraw® Ultra (CambridgeSoft Corp.) computer program was used for simulation of the theoretical isotope distributions. Samples contained Triapine in concentration of 0.10 mM and the $Cu(NO_3)_2$-to-ligand ratio was 1:2 in a nonbuffered aqueous solution; and pH 7.40 was set by the addition of aqueous NH_3 and HNO_3.

Crystallographic Structure Determination: X-ray-diffraction-quality crystals were obtained by slow evaporation of the aqueous solution of Triapine hydrochloride formed in the last step of Triapine synthesis.[8] X-ray diffraction measurements were performed with a Bruker X8 APPEXII CCD diffractometer. A single crystal of suitable size was coated with Paratone-N oil, mounted at room temperature on the tip of a glass fibre and cooled under a stream of cold N_2 maintained by a KRYOFLEX low-temperature apparatus. The crystal was positioned at 40 mm from the detector, and 2390 frames were measured, each for 5 s over 1° scan width. The data were processed with SAINT software.[38] The structure was solved by direct methods and refined by full-matrix least-squares techniques. Non-hydrogen atoms were refined with anisotropic displacement parameters. Hydrogen atoms were placed at calculated positions and refined as riding atoms in the subsequent least-squares model refinements. The isotropic thermal parameters were estimated to be 1.2 times the values of the equivalent isotropic thermal parameters of the atoms to which hydrogen atoms were bound. The following computer programs were used: structure solution (SHELXS-97[39]); refinement (SHELXL-97[40]) molecular diagrams (ORTEP[41]), computer: Pentium® IV; scattering factors.[42] Crystal data and structure refinement details for Triapine·HCl·H_2O are given in Table S2 in the Supporting Information.

CCDC-756635 contains the supplementary crystallographic data for this paper. These data can be obtained free of charge from The Cambridge Crystallographic Data Centre via www.ccdc.cam.ac.uk/data_request/cif.

Supporting Information (see also the footnote on the first page of this article): Figures show EPR and ESI-MS spectra; concentration distribution curves, pH-dependent chemical shifts, and ^1H NMR spectra and crystal data.

Acknowledgments

This work has been supported by the Hungarian Research Foundation OTKA K77833, K72781, F67581 and the Hungarian-Austrian Action Foundation. É. A. E. gratefully acknowledges the financial support of Bolyai J. research fellowships. We thank Zoltán Kele for ESI-MS measurements.

[1] R. B. Singh, H. Ishii, *Crit. Rev. Anal. Chem.* **1991**, *22*, 381–409.
[2] D. X. West, S. B. Padhye, P. B. Sonawane, *Struct. Bonding (Berlin)* **1991**, *76*, 1–50.
[3] a) J. J. Knox, S. J. Hotte, C. Kollmannsberger, E. Winquist, B. Fisher, E. A. Eisenhauer, *Invest. New Drugs* **2007**, *25*, 471–477; b) C. M. Nutting, C. M. L van Herpen, A. B. Miah, S. A. Bhide, J. P. Machiels, J. Buter, C. Kelly, D. de Raucourt, K. J. Harrington, *Annals Oncol.* **2009**, *20*, 1275–1279.
[4] J. Shao, B. Zhou, A. J. Di Bilio, L. Zhu, T. Wang, C. Qi, J. Shih, Y. Yen, *Mol. Cancer Ther.* **2006**, *5*, 586–592.
[5] T. B. Chaston, D. B. Lovejoy, R. N. Watts, D. R. Richardson, *Clin. Cancer Res.* **2003**, *9*, 402–414.
[6] M. Kolberg, K. R. Strand, P. Graff, K. K. Andersson, *Biochim. Biophys. Acta* **2004**, *1699*, 1–34.
[7] R. A. Finch, M. C. Liu, A. H. Cory, J. G. Cory, A. C. Sartorelli, *Adv. Enzyme Regul.* **1999**, *39*, 3–12.
[8] C. R. Kowol, R. Trondl, P. Heffeter, V. B. Arion, M. A. Jakupec, A. Roller, M. Galanski, W. Berger, B. K. Keppler, *J. Med. Chem.* **2009**, *52*, 5032–5043.
[9] D. R. Richardson, P. C. Sharpe, D. B. Lovejoy, D. Senatatne, D. S. Kalinowski, M. Islam, P. V. Bernhardt, *J. Med. Chem.* **2006**, *49*, 6510–6521.
[10] C. R. Kowol, E. Reisner, I. Chiorescu, V. B. Arion, M. Galanski, D. V. Deubel, B. K. Keppler, *Inorg. Chem.* **2008**, *47*, 11032–11047.
[11] D. R. Richardson, D. S. Kalinowski, V. Richardson, P. C. Sharpe, D. B. Lovejoy, M. Islam, P. V. Bernhardt, *J. Med. Chem.* **2009**, *52*, 1459–1470.
[12] a) S. Adsule, V. Barve, D. Chen, F. Ahmed, Q. P. Dou, S. Padhye, F. H. Sarkar, *J. Med. Chem.* **2006**, *49*, 7242–7246; b) F. Bregant, S. Pacor, S. Ghosh, S. K. Chattopadhyah, G. Sava, *Anticancer Res.* **1999**, *19*, 969–972; c) V. M. Leovac, V. S. Jevtovic, L. S. Jovanovic, G. A. Bogdanovic, *J. Serb. Chem. Soc.* **2005**, *70*, 393–422; d) D. Kovala-Demertzi, P. N. Yadav, J. Wiecek, S. Skoulika, T. Varadinova, M. A. Demertzis, *J. Inorg. Biochem.* **2006**, *100*, 1558–1567.
[13] P. V. Bernhardt, P. C. Sharpe, M. Islam, D. B. Lovejoy, D. S. Kalinowski, D. R. Richardson, *J. Med. Chem.* **2009**, *52*, 407–415.
[14] P. D. Bonnitcha, A. L. Vajvere, J. S. Lewis, J. R. Dilworth, *J. Med. Chem.* **2008**, *51*, 2985–2991.
[15] D. X. West, A. E. Liberta, S. B. Padhye, R. C. Chikate, P. B. Sonawane, A. S. Kumbhar, R. G. Yerande, *Coord. Chem. Rev.* **1993**, *123*, 49–71.
[16] S. Padhye, G. B. Kaufmann, *Coord. Chem. Rev.* **1985**, *63*, 127–160.
[17] a) T. S. Lobana, S. Khanna, R. Sharma, G. Hundal, R. Sultana, M. Chaudhary, R. J. Butcher, A. Castineiras, *Cryst. Growth Des.* **2008**, *8*, 1203–1212; b) E. Bermejo, A. Castineiras, I. Garcia-Santos, D. X. West, *Z. Anorg. Allg. Chem.* **2005**, *631*, 2011–2019.
[18] P. Gomez-Saiz, J. Garcia-Tojal, A. Mendia, B. Donnadieu, L. Lezama, J. L. Pizarro, M. I. Arriortua, T. Rojo, *Eur. J. Inorg. Chem.* **2003**, 518–527.
[19] a) M. C. Aguirre, J. Borrás, A. Castineiras, J. M. García-Monteagudo, I. García-Santos, J. Niclós, D. X. West, *Eur. J. Inorg. Chem.* **2006**, 1231–1244; b) A. G. Bingham, H. Boegge, A.

Mueller, E. W. Ainscough, A. M. Brodie, *J. Chem. Soc., Dalton Trans.* **1987**, 493–499.
[20] *SCQuery, The IUPAC Stability Constants Database*, Academic Software (version 5.5), Royal Society of Chemistry, **1993–2005**.
[21] D. J. Leggett, W. A. E. McBryde, *Talanta* **1974**, *21*, 1005–1011.
[22] J. M. Knight, H. Whelan, D. H. Petering, *J. Inorg. Biochem.* **1979**, *11*, 327–338.
[23] a) W. E. Antholine, J. M. Knight, D. H. Ptereing, *Inorg. Chem.* **1977**, *16*, 569–574; b) O. E. Offiong, *Transition Met. Chem.* **1998**, *23*, 553–555.
[24] E. Christofor, F. S. Rojas, J. M. Cano-Pavon, *Talanta* **1991**, *38*, 445–448.
[25] C. R. Kowol, R. Trondl, V. B. Arion, M. A. Jakupec, I. Lichtscheidl, B. K. Keppler, *Dalton Trans.* **2010**, *39*, 704–706.
[26] É. A. Enyedy, unpublished work.
[27] H. Sigel, R. B. Martin, *Chem. Rev.* **1982**, *82*, 385–426.
[28] T. Szabó-Plánka, N. Nagy, A. Rockenbauer, L. Korecz, *Polyhedron* **2000**, *19*, 2049–2057.
[29] a) A. H. Maki, B. R. McGarvey, *J. Chem. Phys.* **1958**, *29*, 31–34; b) B. J. Hathaway, D. E. Billing, *Coord. Chem. Rev.* **1970**, *5*, 143–207; c) A. Rockenbauer, *J. Magn. Reson.* **1979**, *35*, 429–438.
[30] A. Diaz, R. Pogni, R. Cao, R. Basosi, *Inorg. Chim. Acta* **1998**, *275*, 552–556.
[31] R. Pogni, M. C. Baratto, A. Diaz, R. Basosi, *J. Inorg. Biochem.* **2000**, *79*, 333–337.
[32] G. Gran, *Acta Chem. Scand.* **1950**, *4*, 559–577.
[33] H. M. Irving, M. G. Miles, L. D. Pettit, *Anal. Chim. Acta* **1967**, *38*, 475–488.
[34] A. Sabatini, A. Vacca, P. Gans, *Talanta* **1974**, *21*, 53–77.
[35] L. Zékány, I. Nagypál, in: *Computational Methods for the Determination of Stability Constants* (Ed.: D. L. Leggett), Plenum Press, New York, **1985**, pp. 291–353.
[36] A. Rockenbauer, T. Szabó-Plánka, Zs. Árkosi, L. Korecz, *J. Am. Chem. Soc.* **2001**, *123*, 7646–7654.
[37] A. Rockenbauer, L. Korecz, *Appl. Magn. Reson.* **1996**, *10*, 29–43.
[38] *SAINT-Plus* (version 7.06a) and *APEX2*, Bruker-Nonius AXS Inc., **2004**, Madison, Wisconsin, USA.
[39] G. M. Sheldrick, *SHELXS-97*, *Program for Crystal Structure Solution*, University Göttingen, Göttingen, Germany, **1997**.
[40] G. M. Sheldrick, *SHELXL-97*, *Program for Crystal Structure Refinement*, University Göttingen, Göttingen, Germany, **1997**.
[41] G. K. Johnson, *Report ORNL-5138*, Oak Ridge National Laboratory, Oak Ridge, TN, **1976**.
[42] *International Tables for X-ray Crystallography*, Kluwer Academic Press, Dodrecht, The Netherlands, **1992**, vol. C, Tables 4.2.6.8 and 6.1.1.4.

Received: December 4, 2009
Published Online: March 11, 2010

